Evidence for dissolution-reprecipitation of apatite and preferential LREE mobility in carbonatite-derived late-stage hydrothermal processes ⚷

SAM BROOM-FENDLEY[1,2,*], MIKE T. STYLES[2], J. DON APPLETON[2], GUS GUNN[2], AND FRANCES WALL[1]

[1]Camborne School of Mines, University of Exeter, Penryn Campus, Cornwall TR10 9FE, U.K.
[2]British Geological Survey, Nicker Hill, Keyworth, Nottingham, NG12 5GD, U.K.

ABSTRACT

The Tundulu and Kangankunde carbonatite complexes in the Chilwa Alkaline Province, Malawi, contain late-stage, apatite-rich lithologies termed quartz-apatite rocks. Apatite in these rocks can reach up to 90 modal% and displays a distinctive texture of turbid cores and euhedral rims. Previous studies of the paragenesis and rare earth element (REE) content of the apatite suggest that heavy REE (HREE)-enrichment occurred during the late-stages of crystallization. This is a highly unusual occurrence in intrusions that are otherwise light REE (LREE) enriched. In this contribution, the paragenesis and formation of the quartz-apatite rocks from each intrusion is investigated and re-evaluated, supported by new electron microprobe (EPMA) and laser ablation-inductively coupled plasma-mass spectrometry (LA-ICP-MS) data to better understand the mechanism of HREE enrichment. In contrast to the previous work at Tundulu, we recognize three separate stages of apatite formation, comprising an "original" euhedral apatite, "turbid" apatite, and "overgrowths" of euhedral late apatite. The crystallization of synchysite-(Ce) is interpreted to have occurred subsequent to all phases of apatite crystallization. The REE concentrations and distributions in the different minerals vary, but generally higher REE contents are found in later-stage apatite generations. These generations are also more LREE-enriched, relative to apatite that formed earlier. A similar pattern of increasing LREE-enrichment and increased REE concentrations toward later stages of the paragenetic sequence is observed at Kangankunde, where two generations of apatite are observed, the second showing higher REE concentrations, and relatively higher LREE contents.

The changing REE distribution in the apatite, from early to late in the paragenetic sequence, is interpreted to be caused by a combination of dissolution-reprecipitation of the original apatite and the preferential transport of the LREE complexes by F- and Cl-bearing hydrothermal fluids. Successive pulses of these fluids transport the LREE out of the original apatite, preferentially re-precipitating it on the rim. Some LREE remained in solution, precipitating later in the paragenetic sequence, as synchysite-(Ce). The presence of F is supported by the F content of the apatites, and presence of REE-fluorcarbonates. Cl is not detected in the apatite structure, but the role of Cl is suggested from comparison with apatite dissolution experiments, where $CaCl_2$ or NaCl cause the reprecipitation of apatite without associated monazite. This study implies that, despite the typically LREE enriched nature of carbonatites, significant degrees of hydrothermal alteration can lead to certain phases becoming residually enriched in the HREE. Although at Tundulu the LREE-bearing products are re-precipitated relatively close to the REE source, it is possible that extensive hydrothermal activity in other carbonatite complexes could lead to significant, late-stage fractionation of the REE and the formation of HREE minerals.

Keywords: Apatite, carbonatite, rare earth elements, Chilwa Alkaline Province, Tundulu, Kangankunde, REE mobility, dissolution-reprecipitation

INTRODUCTION

Apatite is ubiquitous in carbonatites and can form throughout their genesis, from early magmatic through to late hydrothermal stages (Kapustin 1980; Hogarth 1989). It commonly occurs as fluorapatite in carbonatites, and the term apatite is used synonymously with fluorapatite in this contribution. Apatite has a strong affinity for the REE, with total REE concentra-

tions in those from carbonatite commonly exceeding 1 wt% (Hornig-Kjarsgaard 1998; Bühn et al. 2001). The propensity for the incorporation of REE in apatite means that its behavior in carbonatites can play an important role in their whole-rock REE distribution and the evolution of carbonatites toward REE-rich deposits (Zaitsev et al. 2015). Changes in apatite chemistry can also be used to trace petrological processes in carbonatites and their relationship with associated silicate rocks (e.g., Le Bas and Handley 1979; Stoppa and Liu 1995; Wang et al. 2014). The potential for high REE concentrations in apatite from some carbonatites (e.g., up to 4.9% REE at the Otjisazu carbonatite,

* E-mail: s.l.broom-fendley@ex.ac.uk

Namibia; Hornig-Kjarsgaard 1998) means that it is a mineral of potential economic interest, both as a source of the REE (Mariano and Mariano 2012; Ihlen et al. 2014), as well as a source of phosphorus for direct-application fertilizer (Appleton et al. 1991; Appleton 1994).

Apatite formed in the late-stages of carbonatite emplacement is of particular interest due to its propensity for a HREE content (where HREE includes Eu–Lu + Y; Wall 2014). This type of apatite is uncommon, but has been described in carbonatite complexes at Tundulu, Kangankunde, and Songwe, Malawi; Sukulu, Uganda; and Juquiá, Brazil (Ngwenya 1994; Wall and Mariano 1996; Broom-Fendley et al. 2013; Ting et al. 1994; Walter et al. 1995). In these examples, apatite often displays distinct turbid cores and clear rims, although a fine-grained, anhedral texture is more prominent in the apatite at Sukulu and Songwe. Distinct enrichment in SrO, REE$_2$O$_3$, and Na$_2$O is found in the late stage apatite, that occurs as overgrowths on the earlier-crystallized apatite, that occur as cores or euhedral/ovoid grains. Analyses of apatite from Tundulu and Juquiá show evidence of HREE enrichment in the late-stage apatite rims (Ngwenya 1994; Walter et al. 1995), while Wall and Mariano (1996) described crystallization of xenotime-(Y) in association with the apatite overgrowths at Kangankunde. It is now possible to improve on these studies, which used bulk whole-rock analyses and partial determination of REE contents by EPMA, and aim for a better understanding of HREE enrichment in late-stage apatite. This study explores the hypothesis that late-stage apatite in carbonatites can host the HREE, potentially up to economically significant concentrations. It is also proposed that the variation in REE and trace-element concentration of apatite, through the different paragenetic stages, can be used to infer REE behavior during evolution of the last stages of carbonatite emplacement.

To test the hypotheses proposed above, previously analyzed samples of late-stage apatite from Tundulu and Kangankunde were re-examined. Optical microscopy, cold-cathodoluminescence (CL), and backscattered electron (BSE) imaging were used to decipher the complex parageneses of the apatite at these localities. Spatially resolved REE, major element, and trace element analyses were carried out by EPMA and LA-ICP-MS were acquired to better understand the evolution of REE, Sr, Na, U, and Th from early through to late-stage apatites.

GEOLOGY

Tundulu and Kangankunde are major carbonatite complexes in the Chilwa Alkaline Province (CAP): a late Jurassic–early Cretaceous suite of alkaline rocks and carbonatites in southern Malawi and Mozambique (Garson 1965; Woolley 2001). They are the second and third largest carbonatites in the province, respectively, and each is of particular economic interest for extraction of materials considered as "critical" (Gunn 2014; European Commission 2014), such as the REE and, at Tundulu, apatite.

Tundulu is located approximately 50 km ESE of Zomba, and 25 km NNE of Phalombe, close to the Malawi-Mozambique border (Fig. 1). It comprises three ring structures, the first centered on Tundulu Hill, and the latter two centered on Nathace Hill (Garson 1962; Fig. 1). The first ring structure comprises calcite carbonatite, with varying proportions of subordinate ankerite, apatite, and silicate minerals. Associated rocks include dikes of

nephelinite, melanephelinite, fenite, feldspathic breccias, and agglomerates. The second ring structure comprises calcite carbonatites, apatite-rich calcite carbonatites, quartz-apatite rocks (termed silicified apatite carbonatites by Ngwenya 1994), and ankerite carbonatites (termed bastnäsite carbonatites by Garson 1962), as well as associated alkaline silicate ring dikes (Ngwenya 1991, 1994). The third phase is expressed as a series of alkaline silicate plugs and dikes, variably carbonatized by calcitic and ankeritic fluids.

This study focuses on the quartz-apatite rocks of the second ring structure, predominantly exposed on Nathace Hill (Fig. 1). These rocks are made up of apatite, which can reach up to 90 modal% (Ngwenya 1994), hosted in a quartz groundmass. Subordinate minerals include: hematite; barite; pyrochlore; anatase; rhombic pseudomorphs, filled with calcite and Fe-oxide, most likely after a Fe-carbonate such as siderite or ankerite; and REE-fluorcarbonates. Small-scale mining of this rock type for phosphate fertilizer was observed during fieldwork in 2011 and 2012.

Kangankunde is located 35 km W of Liwonde and 75 km N of Blantyre, just east of the main Blantyre-Lilongwe road (Fig. 1). It is formed of a single large hill, with two small knolls to the north and the south. It predominantly comprises monazite-bearing magnesio- and ferro-carbonatites, mapped as arcuate lobes around the center of the hill (Fig. 1). These have been the subject of various exploration campaigns (e.g., Holt 1965; Dallas et al. 1987). Around the outside of the carbonatite are numerous pods of carbonatite-derived silicified rocks, termed quartz-druse rocks, of different varieties, including monazite-, florencite-, and apatite-rich examples (Garson and Campbell Smith 1965; Wall and Mariano 1996). Cross-cutting relationships and isotope analyses show that these rock types are derived from late stages of carbonatite activity (Garson and Campbell Smith 1965; Wall and Mariano 1996; Wall 2000).

Apatite-rich varieties of these silicified rocks are of particular interest for this study due to their similar habit to rocks from Tundulu. The rocks contain approximately 40% apatite, 40% quartz, and 20% Fe-oxides. On this basis, the rocks have been termed quartz-apatite rocks, using the British Geological Survey (BGS) rock classification scheme (Robertson 1999). Minor xenotime-(Y) mineralization has also been described overgrowing niobian rutile crystals (Wall and Mariano 1996), suggesting possible low tenor HREE enrichment.

SAMPLING AND ANALYTICAL DETAILS

Samples from Tundulu were collected by J.D.A. in 1988 and by S.B.F. in 2011; sampling locations are marked in Figure 1. Sample NHAC was collected from a recently drilled block from the mining operations on Nathace Hill, while the other samples were sourced from outcrop or exploration trenches. A single sample of quartz-apatite rock from Kangankunde was acquired from the Garson collection at the Natural History Museum, London (BM, 1962, 73:131; G1175 in Garson and Campbell Smith 1965). Further sampling of this rock type was attempted (2012), but now no rocks are exposed due to agricultural activity.

Paragenetic relationships were established using optical petrography, cold-CL, and BSE imaging. Cold-CL was carried out at Camborne School of Mines (CSM) using a CITL Mk 3a electron source, operated at ~9 kV and 350 nA, with imagery taken with a 4 s exposure time. BSE imagery was acquired at CSM using a JEOL JSM-5400LV SEM and at the BGS using a FEI Quanta-600 SEM.

Quantitative apatite and REE-fluorcarbonate data were obtained at the BGS using a Link Systems energy-dispersive X-ray (EDS) analyzer on a Cambridge Instruments (CI) Microscan 5 EPMA. Additional apatite data were obtained using a Cameca SX50 using WDS for sample T-160; and an Oxford Instruments X-MAX
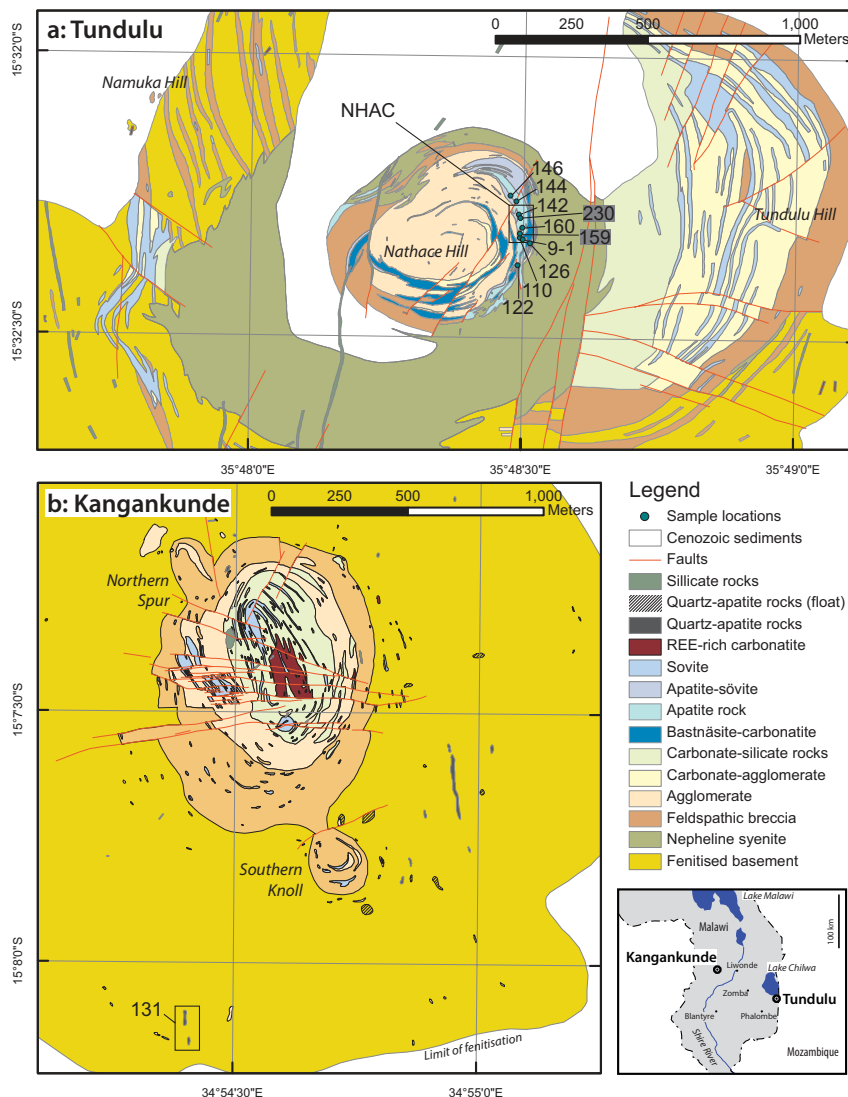
FIGURE 1. Geological maps of Tundulu (**a**) and Kangankunde (**b**) showing sample locations. Inset map shows the location of each carbonatite in southern Malawi. Maps redrawn after Garson (1962) and Garson and Campbell Smith (1965).

large area silicon drift detector EDS system, attached to the FEI Quanta-600 SEM for samples NHAC, T-160, and T-142. Analyses using the CI EPMA were carried out using a 15 kV accelerating voltage and a current of ~5 nA, focused to approximately 4 μm. A range of well-characterized minerals and pure metals were used as standards. Analytical details for the common elements are given by Dunham and Wilkinson (1978), and for the REE by Styles and Young (1983). Quantitative analysis of fluorine was not possible using the CI instrument, although F peaks were detected in all apatite and REE-fluorcarbonate analyses. The limits of detection (LOD) for this instrument are around 0.2 wt% oxide, but higher for the REE: approximately 0.35 wt% oxide. Analyses of sample T-160, using the Cameca EPMA, were carried out using a 15 kV accelerating voltage and a 20 nA current. An electron beam focused to ~0.5 and 5 μm was used and F was analyzed first in the analytical routine, however the difference was small indicating little element migration. Detection limits are between 0.01 and 0.05 wt% oxide, apart from SrO, which is around 0.4% due to interference from Si. Analyses using the FEI EDS system maintained low-intensity beam conditions and short count times (20 kV, 3 nA, and 60 s) to minimize issues arising from F diffusion (Stormer et al. 1993; Stock et al. 2015). Nevertheless, F contents were erratic and should only be considered as semi-quantitative. The 1 μm beam was rastered across an area of approximately 5 × 5 μm to minimize beam damage. Dead-time was typically

around 25%. Quantitative analyses were calibrated using a combination of pure element and mineral standards using the method detailed in Walters et al. (2013). Duplicate analyses of an internal apatite standard using the CI EPMA and, separately, the FEI EDS indicate a relative error of ±1% for these analyses, respectively.

In situ trace element analyses of apatite using LA-ICP-MS was carried out at the BGS. This utilized a New Wave Research Quintupled Nd-YAG 193 nm laser attached to an Agilent-7500 ICP-MS. Single spot analyses, with a diameter of 50 μm, were acquired, maintaining a fluence of approximately 3.5 J/cm^2. Mass numbers analyzed for each element are shown in Supplementary Table 1[1]. Median Ca concentrations for the apatite generation analyzed, obtained by EPMA, were used as the internal standard composition and NIST SRM 610 was used for calibration. SRM 612 was used as a control standard; the concentrations of all analyzed elements are within 10% of the standard values, with most within <5% (Supplemental Fig. 1[1]). Chondrite-normalized REE distributions of repeat analyses of SRM 612 match published values (Supplemental Fig. 2[1]).

---

[1] Deposit item AM-16-35502, Supplementary Figures and Tables. Deposit items are free to all readers and found on the MSA web site, via the specific issue's Table of Contents (go to http://www.minsocam.org/MSA/AmMin/TOC/).

TEXTURAL RELATIONSHIPS

Samples from both carbonatites are characterized by a framework of zoned apatite that comprises distinct anhedral, turbid cores, and euhedral, clear, rim structures (e.g., Fig. 2a). These grains are hosted in a quartz groundmass, with minor associated Fe-bearing carbonate minerals.

Tundulu

As in previous descriptions of apatite from Tundulu (Ngwenya 1991, 1994; Styles 1988), the turbid cores have a spongy texture, with small inclusions of Fe-oxide-rich minerals, and clear rims. Under CL, however, the apatite displays a considerable variety of colors and textures, which can be subdivided
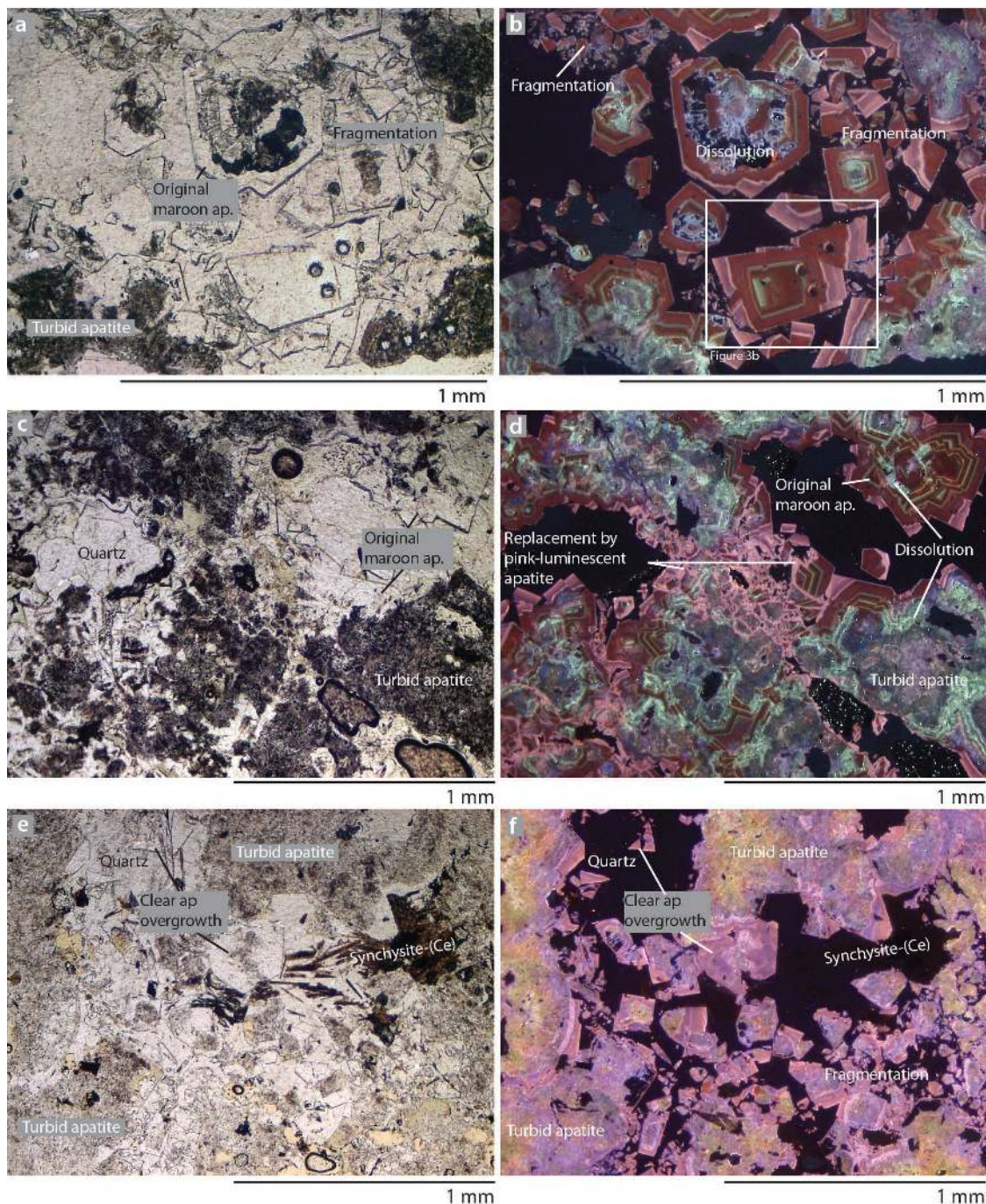

FIGURE 2. Thin-section images under PPL (left) and CL (right) in samples from Tundulu. (**a** and **b**) Early maroon- and green-luminescent apatite undergoing dissolution from the cores outward. (**c** and **d**) The development of pink apatite overgrowths and extensive dissolution leading to the formation of turbid apatite. (**e** and **f**) Extensive dissolution of the original apatite, formation of clear, link-luminescent overgrowths and synchysite-(Ce). Samples T-160: **a–d**, T-159: **e–f**.

into three groups:

(1) "Original," clear, euhedral apatite, which displays concentric zones of maroon- and green-luminescent bands under CL (Figs. 2b and 3a–3b).

(2) "Turbid" apatite, typically forming the anhedral cores of apatite grains and displaying a complex variety of mauve, blue-green, or tan colors under CL (Figs. 2c–2f and 3c).

(3) "Overgrowths," up to 100 μm, of clear, euhedral apatite, which luminesces pink under CL (Figs. 2e–2f and 3a–3b).

In the "original" apatite, the green luminescent zones are considerably smaller (1–10 μm) than the spot size used for LA-ICP-MS, and are therefore grouped with the associated maroon-luminescent zones. This maroon-luminescent apatite can form independent grains up to 500 μm in size (e.g., Figs. 2b and 3b), however, it is most commonly found as small patches with the turbid apatite cores in the center (e.g., Figs. 2b–2d). The turbid cores commonly cross-cut the concentric green and maroon zoning of the maroon-luminescent apatite, indicating that the turbid cores are a replacement product of the original maroon-luminescent apatite. The "original," maroon-luminescent apatite is uncommon at Tundulu, with most of the apatite observed being completely broken-down to a turbid core, with
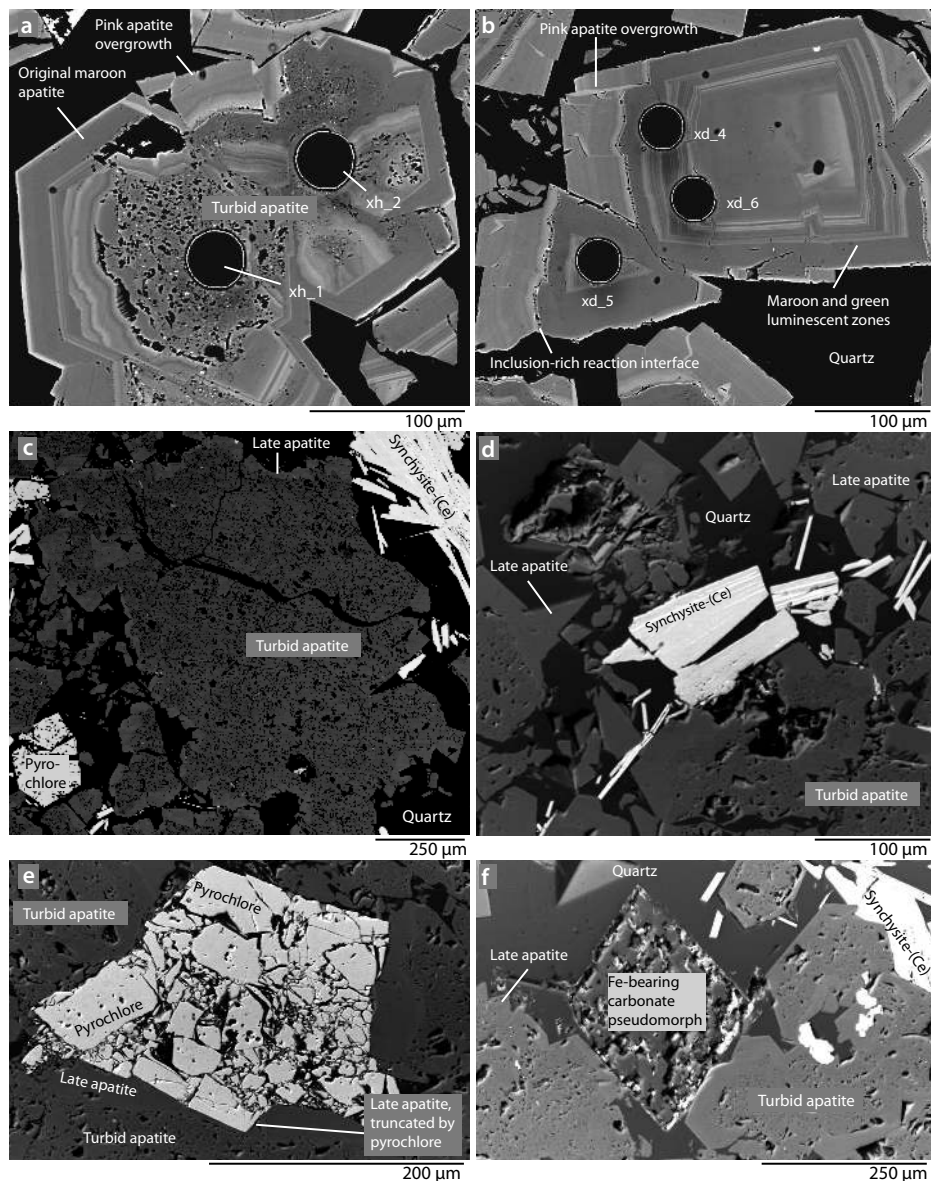

FIGURE 3. BSE images of samples from Tundulu, showing: (**a**) zoning in maroon-luminescent apatite, with dissolution from the core; (**b**) zoning in maroon-luminescent apatite with the development of pink rims; (**c**) extensive dissolution in apatite, with pink luminescent rims, as well as fractured pyrochlore and the formation of synchysite-(Ce) sheaves; (**d**) formation of synchysite-(Ce) sheaves in quartz; (**e**) fragmentation of pyrochlore and evidence of the truncation of apatite rim growth by pyrochlore; and (**f**) pseudomorphs of an Fe-bearing carbonate. Samples T-160: **a–b**, NHAC: **c–f**. Black holes are ablation pits, with analysis numbers corresponding to data in Supplementary Table 3[1].

pink-luminescent, euhedral overgrowths (Figs. 2e–2f). These pink-luminescent overgrowths are found both overgrowing the maroon-luminescent apatite and the turbid apatite and, locally, appear to form along fractures (Fig. 2d). Partial fragmentation of apatite grains, including both cores and rims, is common (Figs. 2b, 2f, and 3c).

Accessory minerals include pyrochlore, rutile, rhombic pseudomorphs after Fe-carbonates, REE-fluorcarbonates, calcite, and quartz. As with the apatite overgrowths, the pyrochlore grains are fragmented (Figs. 3c and 3e). Pyrochlore abuts against the clear apatite rims, but not the turbid cores, indicating formation of pyrochlore prior to the growth of later apatite stages. Calcite and Fe-oxide/hydroxide minerals form in rhombic pseudomorphs (after ankerite or siderite) and, where these are crystallized near apatite, also truncate the apatite rims (Fig. 3f). REE-fluorcarbonates form clean euhedral sheaves, typically 100×200 μm, clumped together and "free floating" in the quartz groundmass (Figs. 2e, 3c, and 3d). These appear undisturbed by brecciation. Quartz is anhedral and fluid inclusions are absent. Minor calcite occurs locally as the groundmass in place of quartz and luminesces bright-orange under CL.
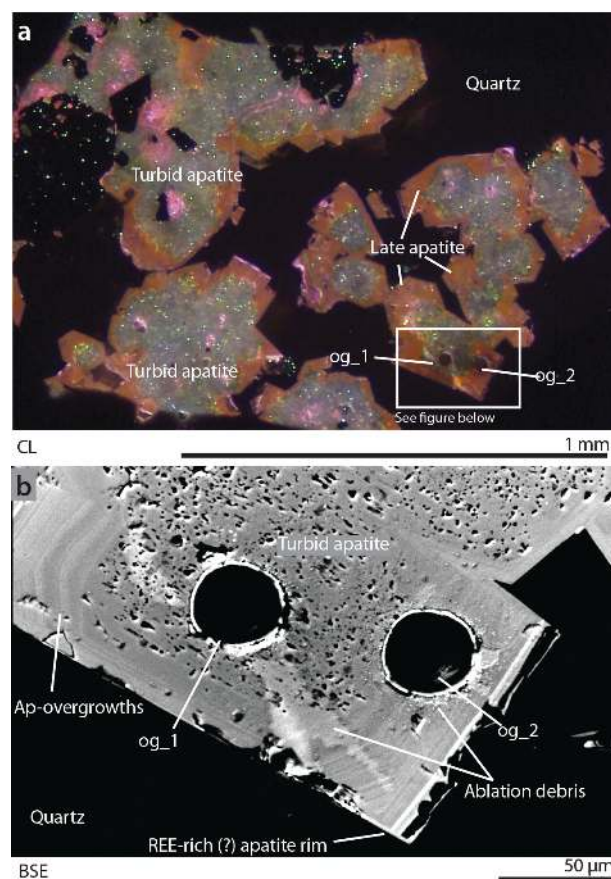

Figure 4. Apatite from Kangankunde sample (BM, 1962, 73:131), showing turbid blue-green cores and orange-brown rims, with pink-luminescent zones randomly distributed (**a**). Fine oscillatory zoning is observable, under BSE, in the orange-brown rims (**b**). Black holes are ablation pits, with analysis numbers corresponding to data in Supplementary Table 3[1].

The minor minerals barite, rhabdophane, and anatase, observed by Ngwenya (1994), were not observed in the samples analyzed for this study, likely due to the small quantities present and analysis of different samples between the studies.

Kangankunde

Apatite from Kangankunde is not as texturally complex as that observed at Tundulu. Two main stages are observed, with blue-green-luminescent turbid cores and orange-brown-luminescent clear rims (Fig. 4a). A pink-luminescent stage is also present, and appears to occur somewhat randomly, distributed both within the cores and on the edges of the grains. Under BSE, fine-scaled oscillatory zoning is common in the rims (Fig. 4b), but is not observable using CL. A bright rim, under BSE, was also observed on the edge of some apatite rims. This is similar to unidentified mid REE (MREE)-rich overgrowths described and analyzed by Wall and Mariano (1996). Rhombic Fe-oxide-rich pseudomorphs after carbonate are common, forming approximately 20% of the rock. These grains truncate the growth of the apatite rims, but appear to have formed at the same time as the turbid cores. REE-fluorcarbonates, as observed at Tundulu, were not found at Kangankunde. Rutile, xenotime, and boulangerite, as described by Wall and Mariano (1996), were not observed in this study.

CHEMICAL COMPOSITION OF APATITE

EPMA and LA-ICP-MS data are presented in Tables 1 and 2. No EPMA data from Kangankunde were collected in this study, and data from Wall and Mariano (1996) are used for comparison.

Tundulu

Turbid cores and clear rims from nine Tundulu samples were analyzed by EPMA. Despite the difference in brightness between the different stages of apatite under BSE, the EPMA data from Tundulu show little compositional variation. P_2O_5 and Na_2O concentrations display a weak negative correlation, with the rims having broadly, although not consistently, higher Na_2O and lower P_2O_5 contents than the cores. Common to apatite from carbonatite, MnO concentrations are low, below the LOD (0.2 wt%) by EDS and only up to 0.1 wt% by WDS, while SrO concentrations are relatively high (<LOD–2%). SiO_2 concentrations are typically below the LOD, while Na_2O contents can approach 2.5 wt%. When analyzed by WDS, the F concentration is sufficiently high (<3 wt%) to indicate that the apatite is fluorapatite.

Turbid cores and euhedral rims, analyzed by LA-ICP-MS, were differentiated by the CL luminescence color of the area analyzed. Using this technique, compositional differences can be discerned. Generally, the pink-luminescent rim analyses have higher concentrations of Na, REE, Th, and Sr than the counterpart turbid cores (Figs. 5 and 6). For example, total REE concentrations range between 8000–20 000 ppm in clear rims and 3000–7000 ppm in turbid cores. Y and Ce, representative of the HREE and LREE, both correlate positively with Na (Fig. 5). This trend is replicated in the Na and Sr data, where concentrations of up to 12 000 ppm are observed in rim analyses, but are typically only ~6000 ppm in the turbid cores (Fig. 6a). U concentrations show no clear difference in concentration in any of the apatite types, and range between 0–150 ppm (Fig. 6e).

TABLE 1. Representative EPMA analyses of Tundulu apatite

Sample	NHAC	NHAC	T-110	T-110	T-121	T-122	T-122	T-142	T-142	T-159	T-159	T-160	T-160	T-230	T-230
Core/Rim	C	R	C	R		C	R	C	R	C	R	C	R	C	R
SOI	8	8						va -1	va -2						
Instrument	FEI	FEI	CI	CI	CI	CI	CI	FEI	FEI	CI	CI	Cameca	Cameca	CI	CI
Representative analyses															
CaO	54.95	53.73	54.93	54.20	53.519	53.31	54.56	52.76	52.43	54.83	53.21	56.43	54.38	54.32	53.13
Na$_2$O	0.35	0.55	0.45	0.67	0.73	0.35	0.85	0.44	0.67	0.58	0.53	0.37	0.92	0.41	0.48
SrO	1.40	1.84	0.97	0.98	1.07	0.52	0.88	1.24	1.32	–	0.97	0.55	1.26	0.78	0.92
FeO	–	–	–	–	–	0.29	–	–	–			0.06	0.05	–	–
Y$_2$O$_3$	–	–	1.04	1.34				0.14	0.29	–	1.18	0.08	0.47	–	–
Ce$_2$O$_3$	–	–						–	0.74			0.05	0.11		
Nd$_2$O$_3$	–	–										0.02	0.17		
P$_2$O$_5$	41.46	40.77	41.41	39.85	40.952	40.43	41.36	42.33	42.14	41.67	40.29	38.99	37.70	40.91	40.77
F	2.73	2.49											3.50		
Total	100.88	99.38	98.79	97.05	93.31	94.90	97.65	96.92	97.60	97.08	96.18	96.52	98.61	96.43	95.30
O=F,Cl	–1.15	–1.05											–1.47		
Total	99.73	98.34											97.14		
Cations per 12.5 O															
Ca	4.839	4.817	4.959	5.016	4.931	4.973	4.960	4.459	4.441	4.978	4.938	5.005	4.991	4.995	4.933
Na	0.056	0.090	0.074	0.113	0.122	0.061	0.139	0.068	0.103	0.095	0.089	0.059	0.152	0.069	0.081
Sr	0.067	0.090	0.047	0.049	0.053	0.053	0.043	0.057	0.061	0.000	0.049	0.026	0.063	0.039	0.046
Fe												0.004	0.003		
Y			0.048	0.063				0.006	0.013		0.056	0.003	0.022		
Ce									0.021			0.001	0.003		
Nd												0.000	0.005		
P	2.885	2.888	2.954	2.913	2.982	2.980	2.971	2.827	2.821	2.990	2.954	2.733	2.734	2.973	2.992
F	0.710	0.659													
Ca site	4.961	4.996	5.129	5.241	5.107	5.079	5.142	4.590	4.639	5.073	5.131	5.101	5.241	5.103	5.061
P site	2.885	2.888	2.954	2.913	2.982	2.980	2.971	2.827	2.821	2.990	2.954	2.733	2.736	2.973	2.992
F site	0.710	0.659													

Notes: – denotes elements below LOD. Blank cells denote elements not analyzed. CI = Cambridge Instruments. Al, Mg, Mn, K, La, Th, Si, S, and Cl are below detection. Full data set available in supplementary information[1].

The oscillatory-zoned, maroon- and green-luminescent apatite from Tundulu has a different chemistry to the other apatite types; it has markedly higher Na contents (9000–15 000 ppm) but without a corresponding increase in other analyzed elements, with the potential exception of Sr (Fig. 6a). While the green-luminescent bands are thinner than the ablation spot size, areas with a high proportion of green-luminescent apatite can be differentiated from the maroon-luminescent apatite. This apatite type has REE concentrations that are equivalent, or lower, than the counterpart turbid apatite, but the green-luminescent zones can have distinctly higher HREE contents, up to 9000 ppm (Fig. 5e). These HREE-rich, green-luminescent bands are interpreted as corresponding to the Y-rich EPMA analyses of Ngwenya (1994; his Table 4, analyses 8 and 12).

Kangankunde

Apatite compositions from Kangankunde and Tundulu share many similarities. Both have low MnO concentrations and comparatively high Na$_2$O and SrO concentrations (Table 1 and Wall and Mariano 1996). In contrast to the data from Tundulu, however, a clear compositional difference between the turbid cores and the clear rims can be observed in the EPMA data, with the latter having much higher SrO concentrations (Wall and Mariano 1996). This difference is reaffirmed by the new LA-ICP-MS data (Fig. 6b), which also shows that there are considerable differences in the REE concentration in comparison with apatite from Tundulu. Y concentrations, for example, are considerably lower at Kangankunde, between 200–800 ppm, while the Ce concentrations are similar, between 0–4000 ppm (Figs. 5a–5d). Relative differences between cores and rims, however, are similar; with the latter having have higher REE,

Th, and U contents. For instance, cores of Kangankunde apatite typically have a REE concentration of approximately 2000 ppm, while rims range between 3000–12 000 ppm (cf. Tundulu: 3000–7000 ppm cores, 8000–20 000 ppm rims).

Chondrite-normalized REE plots

Chondrite-normalized distributions for apatite from each locality are normalized to values from McDonough and Sun (1995). These reflect the differences in Y and Ce concentrations between the two localities (Figs. 7 and 8). The distributions of cores from Kangankunde prominently peak at Sm–Eu, with smoothly decreasing LREE and HREE concentrations. REE patterns for apatite rims from Kangankunde have similar distributions to the cores, but with a higher concentration of the LREE. A negative Y anomaly is observed in both the cores and the rims (Fig. 7).

Maroon- and green-luminescent, concentrically zoned, clear apatite from Tundulu has a variable REE distribution (Fig. 8c). Maroon-luminescent areas are relatively flat in shape, while four analyses that are predominantly green-luminescent display a prominent HREE-enrichment.

Turbid cores from Tundulu generally have higher REE concentrations than those from Kangankunde (note the difference in scale between Figs. 7a and 8b–8f). The distribution patterns of the REE in the turbid cores from Tundulu, however, are highly variable. Few of these distributions are smooth, while some (e.g., Figs. 8b–8d) show a marked break in distribution between Gd and Tb. The different REE distributions in the turbid cores can be divided into:

(1) LREE-poor with a prominent HREE-rich bulge peaking around Y and a very similar distribution to the green-luminescent

TABLE 2. Average and representative LA-ICP-MS analyses of apatite cores and rims from Kangankunde and Tundulu (for full data set see Supplementary Table 3[1])

Location	Tundulu		Tundulu		Tundulu		Kangankunde		Tundulu		Tundulu	
Sample no.	NHAC		T142		T160		BM 1969 131		NHAC		T142	
Point no.	Avg of 16	1 SD	Avg of 25	1 SD	Avg of 16	1 SD	Avg of 10	1 SD	Avg of 11	1 SD	Avg of 23	1 SD
Core/Rim	C		C		C		C		R		R	
Date	2012-12-05		2013-11-21		2013-11-22		2013-11-22		2012-12-05		2013-11-21	
Na	2300	520	3020	830	3440	880	1720	577	3920	890	4200	690
Mg	40	30	90	100	150	140	120	62	80	210	20	30
Mn	160	80	320	280	180	80	820	340	150	90	110	50
Fe	560	260	1640	1960	4200	4250	1300	470	1830	4240	740	720
As			6	3	4	3	2.5	3.4			9	2
Sr	5890	590	6870	1550	6810	1740	8000	6300	8940	2230	8800	1530
Y	1940	620	1680	570	2220	800	320	180	3340	860	2760	1010
Zr			360	430	370	300	1000	480			70	300
Ba	260	220	250	180	370	310	320	140	210	210	70	100
La	480	270	420	300	70	60	140	270	930	440	720	270
Ce	1250	570	1090	690	170	120	540	940	2400	1030	1890	510
Pr	180	60	150	90	30	20	81	130	330	110	280	70
Nd	900	230	700	430	140	110	460	710	1690	550	1500	420
Sm	260	200	200	130	70	60	200	250	550	220	580	250
Eu	102	97	74	48	39	30	67	73	219	86	225	104
Gd	313	305	224	144	144	94	170	170	673	272	683	332
Tb	59	41	44	20	42	26	19	15	118	39	107	42
Dy	384	171	309	116	323	161	84	56	713	199	617	251
Ho	74	25	63	22	81	28	11	6.7	127	33	103	35
Er	173	42	158	57	229	75	24	12	270	64	213	67
Tm	20	4	19	8	29	11	3.2	1.6	27	7	21	6
Yb	104	24	95	40	154	54	22	11	124	34	87	22
Lu	12	3	10	4	16	6	3.5	1.8	12	4	8	2
Pb	9	5	14	15	7	3	99	18	15	14	8	4
Th	247	194	188	206	87	136	220	210	705	475	403	273
U	16	7	20	23	33	25	6.3	5.7	28	15	17	18

Location	Tundulu	Tundulu	Tundulu	Tundulu		Tundulu		Kangankunde	
Sample no.	T142	T142	T160	T160		T160		BM 1969 131	
Point no.	vc-4[a]	ve-6[a]	xh-2[a]	Avg of 6	1 SD	Avg of 4	1 SD	Avg of 10	1 SD
Core/Rim	Maroon CL	Maroon CL	R	Maroon CL		Green CL		R	
Date	2013-11-21	2013-11-21	2013-11-22	2013-11-21		2013-11-21		2013-11-22	
Na	7410	8820	2850	9910	1940	11060	2280	3440	586
Mg	30	160	20	220	220	320	220	74	76
Mn	230	510	140	450	240	380	70	734	355
Fe	850	2030	600	2000	720	2580	790	1020	1050
As	9	6	0	2	1	1	0	10	4
Sr	9990	7090	11200	10020	1800	7630	100	16200	4950
Y	2440	2110	300	960	390	4680	1560	574	328
Zr	60	1130	120	960	610	760	360	257	176
Ba	50	320	830	150	50	230	60	170	110
La	770	810	90	210	90	50	20	780	310
Ce	2080	1970	140	460	230	120	70	2700	1000
Pr	280	240	20	60	30	20	10	400	150
Nd	1540	1110	50	260	180	130	110	2200	910
Sm	460	300	10	80	80	90	70	810	290
Eu	182	113	6	38	36	66	30	250	92
Gd	532	320	19	120	110	301	100	580	210
Tb	79	63	5	25	19	111	35	51	22
Dy	524	432	43	170	98	889	283	180	96
Ho	78	86	11	36	16	184	58	21	12
Er	183	198	29	96	23	419	102	37	21
Tm	17	23	4	14	2	44	7	3.9	1.8
Yb	74	115	27	95	32	214	16	23	7.9
Lu	8	12	4	13	5	21	2	3	0.9
Pb	11	19	27	53	36	17	18	100	23
Th	332	558	39	204	112	377	444	610	191
U	12	58	7	60	48	49	37	5.3	2.5

Notes: bd = below detection; Nb, Si, K, Ti, and Cd all below detection. Blank cells denote elements not analyzed. Concentrations in parts per million.
[a] Representative analyses.

bands in the clear apatite (Fig. 8a). This distribution pattern displays both positive and negative Y anomalies (Fig. 8b).

(2) Relatively flat, LREE-rich, but with a distinct enrichment in the MREE/HREE, starting at Gd and peaking at approximately Y. Most analyses have a minor negative Y anomaly, and some have a small positive Eu anomaly (Fig. 8c).

(3) Relatively flat, LREE-rich, HREE-poor, with a small Y anomaly (Fig. 8d).

(4) A convex-up curved distribution, peaking at the MREE, around Gd and a minor Y anomaly. Most analyses have this distribution (Fig. 8e).

Pink-luminescent rims from Tundulu are broadly LREE–MREE enriched, peaking at Sm–Eu, with steeply sloping distributions at the HREE end of the diagram (Fig. 8b).
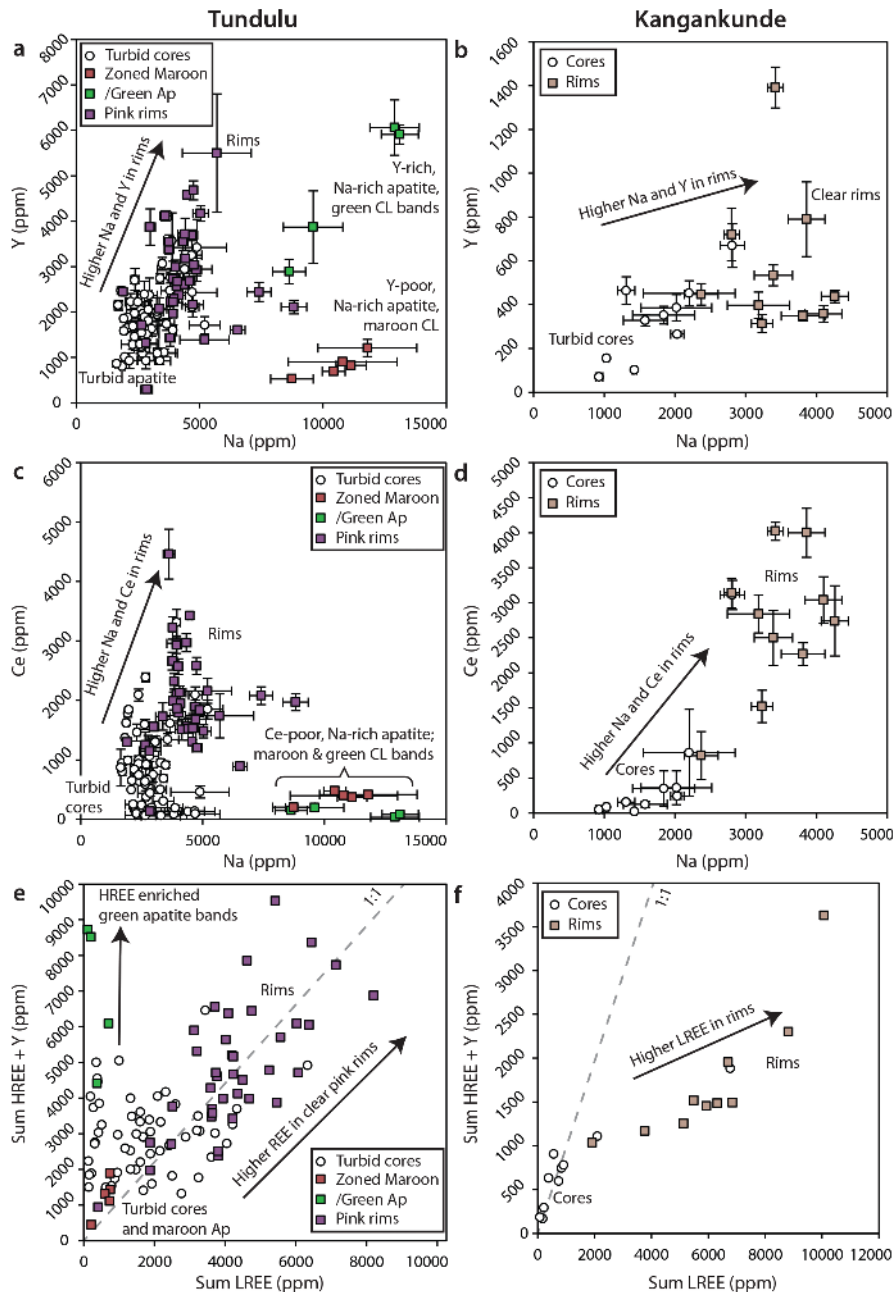
FIGURE 5. Binary plots of REE and Na LA-ICP-MS data from the cores and rims of apatite from Tundulu (**a**, **c**, **e**) and Kangankunde (**b**, **d**, **f**). The color of the symbols for the rim data are representative of the CL luminescence color. Pink rims from Tundulu, and orange-brown rims from Kangankunde, have associated enrichments in Na, Y, and Ce. Maroon-luminescent rims from Tundulu have high Na concentrations, but little attendant REE enrichment.

Included for reference, on each chondrite-normalized plot, is a summary of a range of data from carbonatite-derived apatite from other carbonatite complexes (compiled from Hornig-Kjarsgaard 1998; Bühn et al. 2001; Brassinnes et al. 2005; Chen and Simonetti 2013; and Zaitsev et al. 2015). This comparison highlights

the contrast between the REE distributions of apatite formed at most carbonatites, typically from a carbonatite melt, and the distribution of the late-stage apatite in this study. Commonly, apatite derived from carbonatite has a strongly LREE-enriched distribution, with a linear decrease in HREE concentrations. A negative Y anomaly is also apparent. Comparison of distributions between the Kangankunde analyses and the published data indicates many broad similarities, such as a generally LREE-rich distribution. Most notably different, however, is the prominent peak in Sm–Eu, which is atypical of carbonatite-derived apatite. REE distributions of Tundulu apatite are markedly different from the compiled data set, with all analyses displaying higher MREE and HREE contents. REE concentrations in the pink-luminescent rims are also relatively high, compared to most carbonatite-derived apatite.

CHEMICAL COMPOSITION OF REE-FLUORCARBONATES

EPMA analyses of REE-fluorcarbonates from five Tundulu samples are presented in Table 3. These REE-fluorcarbonate grains are typical of those found in the quartz-apatite rock. These were analyzed by EDS, and the elements F and C could not be determined. The matrix correction was made assuming oxygen is present in stoichiometric proportions to the cations detected, hence the ionic formulas are reported on the basis of 7.5 O (Table 3). Treating all the undetected elements in the matrix as O will lead to some errors but as they have similar atomic numbers and C is lower and F is higher the overall error is thought to be small. The results with formulas close to the ideal formula support this assumption.

The main mineral present is synchysite-(Ce), owing to its high Ca contents. This shows 6 cations on the basis of 7.5 O, of which 3 are Ca, and just fewer than 3 are the REE, allowing for the heavier REE, which were not analyzed. This ratio corresponds to an idealized formula of $Ca_3Ce_3(CO_3)_6F_3$, allowing for the fact that C and F were not detected. Chondrite-normalized plots show that the synchysite-(Ce) is strongly LREE-enriched, common to REE-fluorcarbonates (Supplemental Fig. 4[1]).
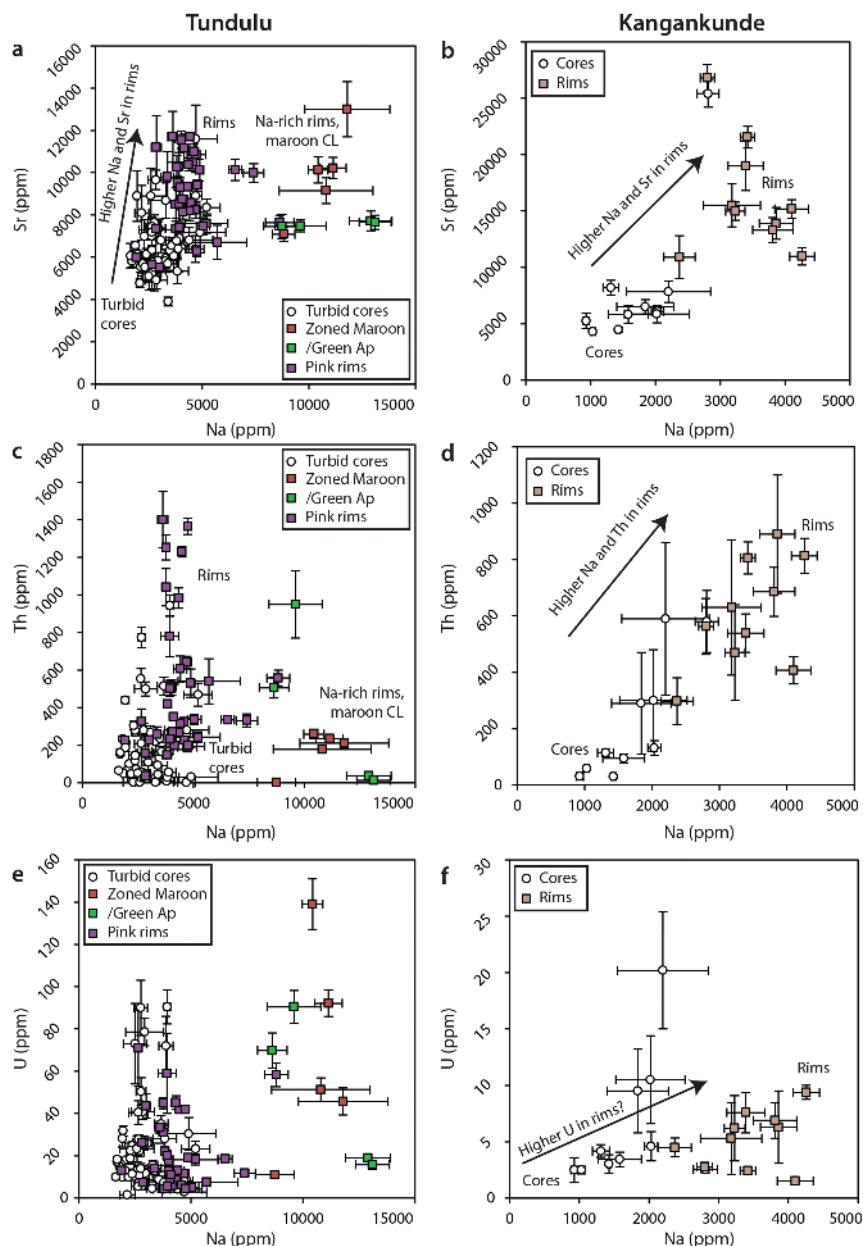
FIGURE 6. Binary plots of Sr, U, and Th LA-ICP-MS data. Symbol colors are the same as Figure 5. The pink rims from Tundulu and orange-brown rims from Kangankunde have associated enrichments in Na, Sr, and Th. Maroon rims from Tundulu have, in some samples, increased Sr concentrations.

DISCUSSION

Paragenetic interpretation

Mechanisms to explain the very high abundances of apatite at Tundulu and Kangankunde are unknown. The occurrence of the rock type in concentric bands around the main vent at Tundulu suggests that it could have formed as a cumulate. However, while equivalent rocks can be found near the main intrusion at Kangankunde, most are found in bands around the outside of the carbonatite, up to 1 km from the center of the intrusion (Fig. 1). This distance from the center, and the abundance of quartz in the rock matrix, commonly associated with the late stages of carbonatite intrusion (e.g., Le Bas 1989), attests to the formation of these rocks from a hydrothermal fluid, which is highly likely to be associated with the carbonatite magmatism. This is further supported by the positive $\delta^{18}O$ values (12–17 ‰ SMOW) in the quartz-rocks at Kangankunde, estimated to be equivalent to a formation temperature of 230 °C (Wall 2000). The similar habit of the quartz-apatite rocks at Kangankunde and Tundulu suggests a common mode of formation, likely to be from carbonatite-derived hydrothermal fluids. The paragenesis of the quartz-apatite rocks from each locality has been reassessed, using the new textural data and assuming a hydrothermal formation.

Tundulu. At Tundulu, Ngwenya (1991, 1994) interpreted the paragenesis and suggested that rhabdophane (not identified in this study) and synchysite-(Ce), both LREE-rich minerals, formed early. This was followed by apatite, barite and, finally, quartz (Fig. 9a). This early formation of synchysite-(Ce) and late apatite crystallization was proposed to be compatible with the assumption that HREE enrichment in the later apatite required prior LREE removal from a fluid. This was suggested to have been caused by the prior crystallization of LREE-minerals, including synchysite-(Ce). However, the petrographic observations of this study indicate that apatite overgrowths do not enclose or surround synchysite-(Ce), suggesting that synchysite-(Ce) was not present during the growth of the apatite (e.g., Figs. 2e and 3c–3d). Furthermore, while all the different apatite generations are brecciated, no brecciation is observed in the synchysite-(Ce). This indicates that apatite crystallized before synchysite-(Ce) and a revised explanation is required.

In this new model, clear euhedral grains of oscillatory-zoned, green- and maroon-luminescent apatite are interpreted as forming early, cogenetic with pyrochlore and Fe-bearing carbonate. This is based on their euhedral oscillatory growth zones, and subsequent dissolution and overgrowths. Breakdown and dissolution of apatite from preceding stages is inferred by the presence of turbid cores cross-cutting concentric green- and maroon-luminescent bands (e.g., Figs. 2b–2d), embayed maroon-luminescent zones and the
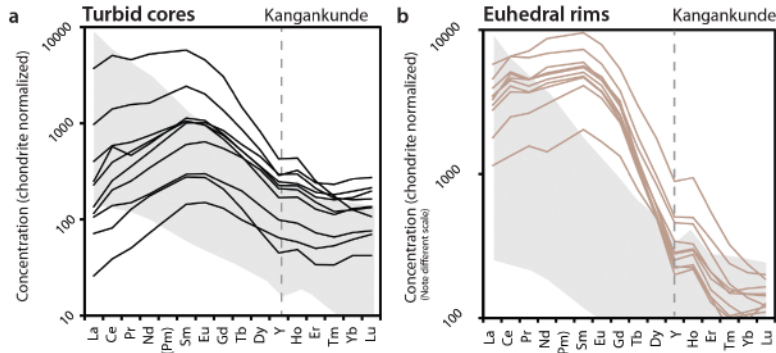
FIGURE 7. Chondrite-normalized distributions for apatite turbid cores and clear rims from Kangankunde. Line colors represent the color of apatite luminescence under CL. Chondrite values from McDonough and Sun (1995).
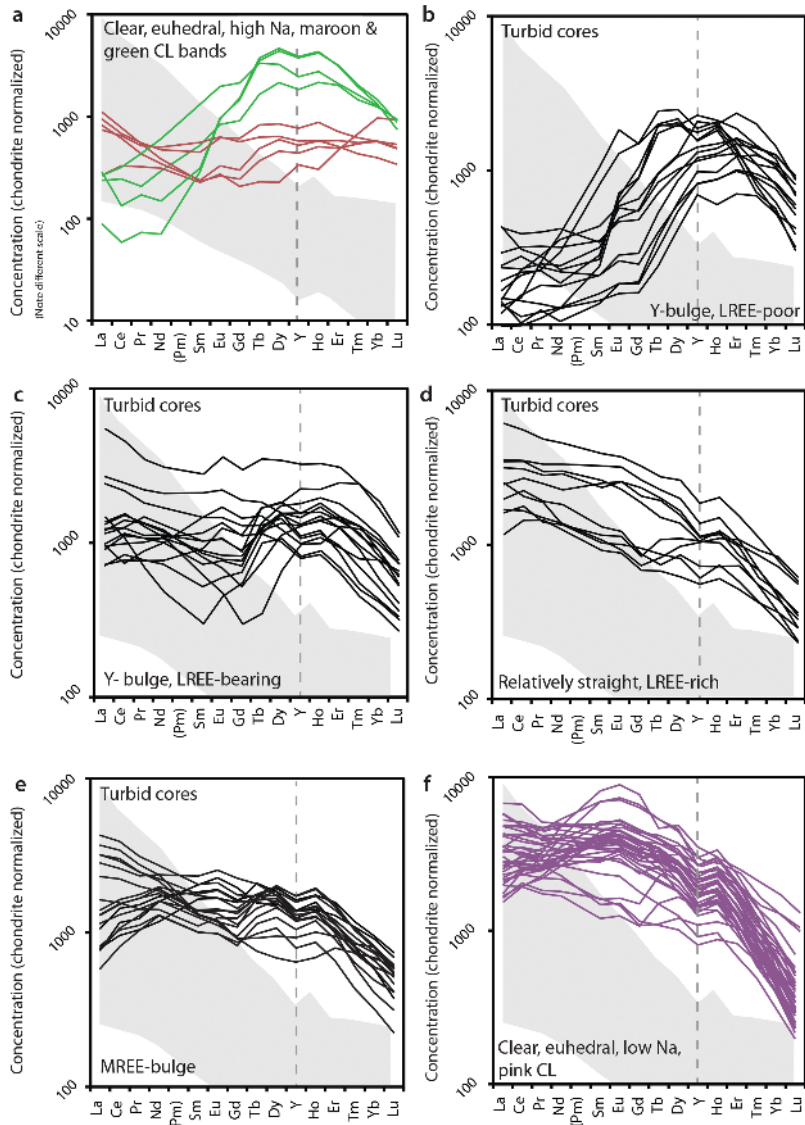

FIGURE 8. Chondrite-normalized REE distributions for "original" apatite (**a**) turbid apatite cores (**b**–**e**) and rims (**f**) from Tundulu. The distributions from Tundulu cores are split to aid visualization. Yttrium is highlighted for clarity. Line colors in **a** and **f** represent the color of apatite luminescence under CL. No color consistency is noted in core analyses (**b**–**e**) and these are only separated for clarity between the different distribution types. Chondrite values from McDonough and Sun (1995).

TABLE 3.   Synchysite-(Ce) analyses from Tundulu by EPMA (CI instrument)

| Sample	T-9-1	T-9-1	T-122	T-122	T-122	T-122	T-126	T-126	T-126	T-142	T-142	T-142	T-146	T-146
Analysis number	7	10	1	3	4	5	2	3	4	1	2	3	6	9
CaO	16.94	16.23	16.40	16.92	16.34	17.04	15.95	15.97	16.82	16.05	17.47	17.53	16.71	17.12
SrO	0.99	bd	0.68	0.94	1.08	1.04	0.26	0.72	0.69	0.55	0.97	1.07	1.02	1.16
La_2O_3	14.73	18.68	13.23	15.72	13.65	14.10	11.86	9.37	13.67	14.39	15.24	14.48	13.84	13.31
Ce_2O_3	27.03	23.99	25.34	26.45	24.93	24.28	21.94	20.02	22.59	24.31	25.71	24.24	23.34	22.89
Pr_2O_3	1.85	bd	1.41	1.50	bd	1.81	2.01	1.33	bd	1.28	2.24	1.57	1.38	2.16
Nd_2O_3	5.32	3.60	4.75	4.64	5.49	5.66	7.05	8.85	6.16	5.73	6.14	6.28	6.18	6.32
ThO_2	0.78	bd	bd	bd	bd	bd	1.12	2.38	0.73	0.79	0.68	1.08	bd	bd
Total	67.63	62.51	61.81	66.16	61.49	63.93	60.18	58.64	60.66	63.10	69.04	66.24	62.46	62.95
Total REE	48.93	46.28	44.72	48.30	44.08	45.85	42.86	39.57	42.42	45.71	49.33	46.56	44.74	44.67
Number of cations on the basis of 7.5 O														
Ca	2.963	3.045	3.100	3.008	3.103	3.110	3.109	3.188	3.217	3.002	2.972	3.100	3.120	3.161
Sr	0.093		0.070	0.091	0.110	0.103	0.027	0.078	0.071	0.056	0.089	0.102	0.103	0.116
La	0.887	1.207	0.861	0.962	0.892	0.886	0.796	0.644	0.900	0.927	0.893	0.882	0.890	0.846
Ce	1.616	1.538	1.637	1.607	1.618	1.515	1.461	1.365	1.476	1.554	1.495	1.465	1.489	1.445
Pr	0.110		0.090	0.090		0.112	0.133	0.091		0.081	0.130	0.094	0.087	0.136
Nd	0.310	0.225	0.299	0.275	0.348	0.344	0.458	0.589	0.393	0.357	0.348	0.370	0.385	0.389
Th	0.029						0.046	0.101	0.030	0.031	0.024	0.041		
Total	6.01	6.01	6.06	6.03	6.07	6.07	6.03	6.06	6.09	6.01	6.13	6.05	6.07	6.09
Total REE	2.92	2.97	2.89	2.93	2.86	2.86	2.85	2.69	2.77	2.92	2.87	2.81	2.85	2.81

Notes: Na_2O not detected except for T-142 analysis 2. Y_2O_3 below detection. bd = below detection.

absence of maroon-luminescent apatite in most samples (e.g., Fig. 2f). Growth of the pink-luminescent apatite rims followed these stages, or was synchronous with dissolution, as clearly indicated by the truncation of apatite rims by pyrochlore and carbonates (Figs. 3e–3f). This gives the order: crystallization of maroon and green (luminescing) apatite → dissolution of maroon and green apatite → reprecipitation as pink rims. Fragmentation and brecciation of apatite and pyrochlore indicates that a minor brecciation event occurred after the formation of these minerals (e.g., Figs. 2, 3c, and 3e). Pink-luminescent apatite locally overgrows brecciated turbid and maroon apatite indicating that brecciation was synchronous with the formation of the pink-luminescent rims (Fig. 2d). However, this relationship is uncommon, and in most samples pink-luminescent apatite is also brecciated (e.g., Fig. 2f). The REE-fluorcarbonates appear undisturbed by brecciation, often forming solid 100–200 μm "booklets" (Figs. 3c–3d), and are always in the interstices between the apatites. This indicates that these crystallized after the fragmentation of the apatite and pyrochlore. Mineralization terminated with the crystallization of the groundmass of anhedral quartz and minor calcite.

Kangankunde. In the quartz-apatite rock from Kangankunde, Wall and Mariano (1996) interpreted the turbid apatite cores as forming first. This was followed by apatite overgrowths, co-crystallizing xenotime and Fe-carbonates (subsequently weathered), a REE-rich phosphate stage and, finally, quartz. The petrography carried out in this study supports this interpretation, although xenotime was not identified, likely due to the rarity of this mineral.

Apatite substitution mechanisms

The REE commonly substitute into apatite via a charge-balancing coupled substitution, usually with SiO_4^{4-} or Na^+, into the PO_4^{3-} or Ca^{2+} sites, respectively (Pan and Fleet 2002; Hughes and Rakovan 2015):

$$REE^{3+} + SiO_4^{4-} = Ca^{2+} + PO_4^{3-} \tag{1}$$
$$REE^{3+} + Na^+ = 2Ca^{2+} \tag{2}$$
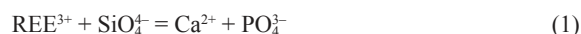
Given the correlation between the REE and Na (Figs. 5a–5d), and the low SiO_2 concentration from apatite at both Kangankunde

and Tundulu (Table 1), it is highly likely that Na^+ (Eq. 2) is responsible for charge-balancing the substitution of the REE in both the core and rim analyses.

High Na concentrations in the maroon-luminescent apatite from Tundulu do not correlate with any of the other analyzed elements, with the possible exception of Sr (Fig. 6a). Apatite cannot be significantly charge imbalanced, and another, unanalyzed, element(s) must be substituting. Possible substitutions to balance the Na^+ substitution include coupled substitutions with: 3^+ cations other than the REE; SO_4^{2-}; CO_3^{2-}; and F^-, with the corresponding formation of a vacancy (Pan and Fleet 2002). The substitution of other 3^+ cations for Ca^{2+}, such as Bi^{3+} and Cr^{3+}, are known in synthetic apatite but these are unlikely to occur in nature and have not been documented in apatite from other carbonatites (e.g., Hornig-Kjarsgaard 1998; Chen and Simonetti 2013; Xu et al. 2010; Bühn et al. 2001). SO_4^{2-} substitution is also unlikely as, where analyzed, S is below the EPMA LOD.

Considerable significance is given to the possibility of CO_3 substituting for PO_4 due to the presence of CO_3 adsorption lines in a bulk-apatite infrared spectrum (Styles 1988; Supplemental Fig. 3[1]). This is from a sample that predominantly comprises clear apatite, largely of the maroon-luminescent variety (T-160), which is considered to be "original." It does, however, also contain a minor component of pink-luminescent clear apatite (T-159), and a potential contribution from CO_3 in this apatite type cannot be fully excluded. However, this apatite type is not charge imbalanced, and it is more likely that the CO_3 is hosted in the clear, maroon-luminescent "original" apatite.

Substitution of CO_3 for PO_4 is documented from other carbonatites, where CO_2 concentrations can reach up to 1.9 wt% (Binder and Troll 1989; Liu and Comodi 1993; Brigatti et al. 2004). CO_3 substitution in the maroon-luminescent apatite is also supported by the negative correlation between PO_4 and Na_2O in the EPMA data (Table 1), suggesting that CO_3 is substituting in the PO_4 site through type B substitution (Fleet et al. 2004). The analytical difficulty involved in analyzing F in apatite (e.g., Stormer et al. 1993; Stock et al. 2015), however, means that the substitution of F^-, with the formation of a vacancy, as a mechanism for balancing higher Na contents, cannot be excluded.
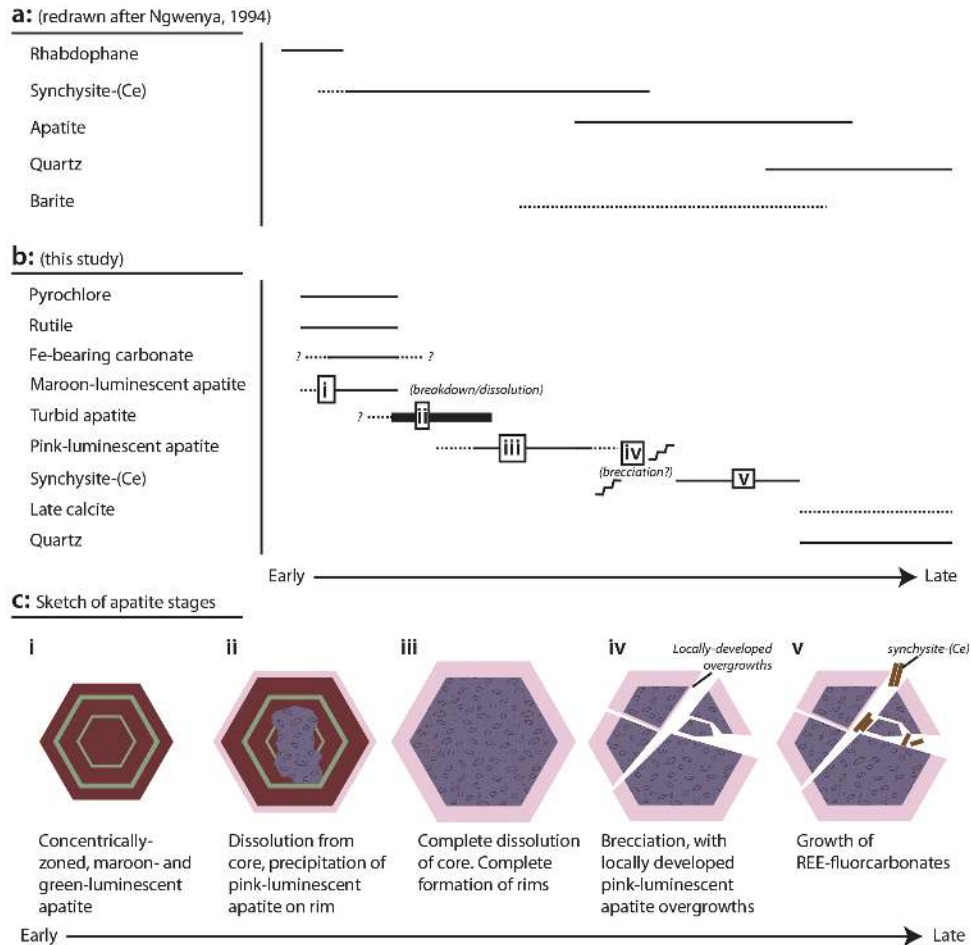
FIGURE 9. Interpretations of the paragenetic sequence at Tundulu: (**a**) redrawn after Ngwenya (1991, 1994); (**b**) this study. Roman numerals correspond to sketches in **c**, representing the different paragenetic stages of apatite observed at Tundulu.

Apatite as a host for the HREE?

Apatite has been mooted as a potential source of the REE (Mariano and Mariano 2012; Ihlen et al. 2014), and apatite with enriched HREE tenors could be attractive for REE extraction. Previous analyses of apatite from the study areas, using EPMA, have noted an increase in the HREE quotient of the rims. In the case of Tundulu, Ngwenya (1994) described a fourfold increase in Y over Ce, while Wall and Mariano (1996) noted an increase in the MREE concentration in the latest phosphate stages. HREE-enrichment is rare, especially in carbonatite-derived rocks, which are characteristically LREE-enriched (e.g., comparison data in Figs. 7 and 8). It is therefore of interest to confirm these REE distributions and to constrain the mechanism for HREE enrichment so that HREE-enriched apatite can be targeted at other carbonatite complexes.

The results of this study confirm that apatite, which formed later in the paragenetic sequence, has higher concentrations of the REE as a whole, with total REE contents reaching ~15 000 ppm (Fig. 5e). However, the re-interpretation of the paragenesis at Tundulu indicates that HREE enrichment does not occur late. Rather, HREE enriched distributions are only observed in early apatite. This includes both the green-luminescent bands in the

early "original" apatite, where HREE contents can reach 9000 ppm, and in the turbid apatite. HREE enrichment in the turbid apatite is varied, and has low REE concentrations, with HREE contents attaining a maximum of approximately 5000 ppm. In contrast, chondrite-normalized distributions for the rims are consistently M/LREE enriched and the ratio between the LREE to the HREE, in terms of absolute concentration, remains approximately 1:1 for both earlier turbid cores and later euhedral rims (Fig. 5e). At Kangankunde, chondrite normalized distributions between cores and rims are similar (Fig. 7). However, while analyses of cores typically have approximately 1:1 ratios of LREE:HREE, rim analyses have a much greater relative concentration of the LREE, with a ratio of approximately 4:1 (Fig. 5f).

How is apatite HREE-enriched?

The previous model for HREE-enrichment in late apatite at Tundulu involved preferential partitioning of the LREE into early crystallizing synchysite, with the residual HREE partitioning into the later-crystallizing apatite (Ngwenya 1994). The revised paragenesis means that this mechanism is no longer tenable, and a new one is proposed. We suggest that a combination of

dissolution-reprecipitation and preferential LREE mobility led to the release of REE from the "original" apatite and the sequestering of the LREE within newly formed apatite rims. Some LREE remained in solution, crystallizing later in the paragenetic sequence as synchysite-(Ce).

Dissolution-reprecipitation of apatite. Dissolution-reprecipitation is a reaction, in the presence of a fluid, replacing an original phase with either an entirely new phase, or the same phase with a different composition, to reduce the free energy of a system (Putnis 2002, 2009; Ruiz-Agudo et al. 2014). A corresponding volume decrease promotes porosity/permeability generation and the potential for further dissolution. Despite its relatively low solubility (Ayers and Watson 1991), dissolution-reprecipitation of apatite has been observed in several natural samples [e.g., Kiruna-type apatite-magnetite deposits (Harlov et al. 2002a, 2005), metagabbro (Engvik et al. 2009), nepheline-clinopyroxenites (Krause et al. 2013)]. It has also been recreated experimentally under a ranges of pressures and temperatures (300–900 °C, 500–1000 MPa), in the presence of H_2O; NaCl-, KCl-, and $CaCl_2$-bearing brines; H_2O/CO_2 mixtures; HCl; and H_2SO_4 (Harlov et al. 2002b, 2005; Harlov and Förster 2003).

Some of the textural criteria for dissolution-reprecipitation, as outlined by Putnis (2009), are applicable to the apatite at Tundulu and Kangankunde. These include: (1) a close spatial relationship between the parent and product phases; and (2) a sharp reaction front between parent and product. This is indicated by the development of the pink-luminescent product apatite on the rim of the turbid reactant apatite, and the presence of an inclusion-rich boundary layer (Figs. 3a and 3b) between the reactant and product phases.

Porosity (or permeability) development is a common feature of dissolution-reprecipitation, necessary for the propagation of further dissolution within the mineral (Putnis and Ruiz-Agudo 2013). In documented examples, this always forms in the product phase (e.g., Putnis 2009), but at Tundulu and Kangankunde significant porosity is also present in the reactant phase (e.g., Figs. 2 and 3). The reasons for this are unknown, but a possible cause is the potentially higher CO_3 concentration in the "original" apatite, which may be more susceptible to dissolution, and concomitant volume change.

Despite the unusual development of porosity within the core of the apatite grains, the turbid nature of the cores is persuasive evidence for dissolution. Development of pink-luminescent rims, in close proximity to the zone of dissolution, strongly suggests that these formed from rapid re-precipitation of phosphorus, derived from the dissolved turbid apatite. Likewise, at Kangankunde, similar, albeit simpler, dissolution-reprecipitation process can be inferred, with the turbid cores as the reactant phase and the formation of clear, euhedral rims as a product phase.

Preferential LREE mobility. Cores of the apatite are HREE-enriched and rims are LREE-enriched. This difference in composition between the turbid, reactant apatite and clear, euhedral, product apatite can be used to infer the relative mobility of the REE, assuming that the source of at least some of the REE is the original apatite. At Tundulu, "original" clear apatite is M/HREE-enriched (Fig. 8a), with relatively low REE contents. Turbid, reactant apatite displays a range of REE distributions, but many are HREE-enriched (Figs. 8b–8e). This apatite type commonly also has relatively low REE contents. Clear, euhedral, product apatite is

M/LREE-enriched (Fig. 8f). This apatite type commonly has the highest relative REE concentration. Furthermore, these subsequent apatite generations are paragenetically followed by the formation of synchysite-(Ce), with a LREE-rich distribution (Supplemental Fig. 4[1]). At Kangankunde, the REE distributions between early, reactant apatite, and late, product apatite are similar. However, the LREE concentration in the product apatite is relatively greater than that of the reactant apatite (Fig. 5f).

These sequential changes in REE distribution, from early and HREE-rich, through to late and LREE-rich, could be caused by the different stability of the different REE in solution. This would depend on which anion, or anions, are complexing the REE. The REE can be transported in hydrothermal fluids, as chloride-, fluoride-, sulfate-, or carbonate-complexes (Haas et al. 1995). Recent experimental work on the stability of REE-chloride and -fluoride complexes, at elevated temperature, has shown that the LREE complexes are more stable than their HREE counterparts (Migdisov et al. 2009; Williams-Jones et al. 2012; Migdisov and Williams-Jones 2014). Limited work on REE-sulfate complexes indicates that there is little difference in the relative stability of the LREE and HREE (Migdisov and Williams-Jones 2008), while no experimental work has been carried out on REE-carbonate complexes. Given the relative differences in the stabilities of REE-chloride and fluoride complexes, if the large volumes of fluid required for extensive apatite dissolution are Cl- or F-bearing, the LREE would be preferentially mobilized over the HREE. This process has been conceptually modeled for the Nechalacho REE deposit, Canada, where eudialyte has been metasomatically replaced by zircon and other REE-bearing minerals (Sheard et al. 2012). Successive aliquots of REE- and Cl-bearing fluid were passed through a phosphate-bearing rock, leading to LREE-transport and removal (Williams-Jones et al. 2012). This results in passive relative enrichment of the residual HREE at the source. A similar process is inferred to have taken place in the quartz-apatite rocks at Kangankunde and Tundulu. Dissolution of "original" apatite releases REE from the apatite structure and the REE are complexed by Cl (or F). The relatively lower stability of $HREECl^{2-}$, over the equivalent LREE complex, leads to the retention of the HREE in the turbid cores of the apatite, while the M/LREE are transported somewhat further to the clear, euhedral apatite rims. The most stable LREE are retained in solution, forming the late-stage synchysite-(Ce).

The variety of REE distributions for turbid apatite is suggested to be a function of different degrees of dissolution, as well as a function of the composition of the original apatite. Greater degrees of dissolution are likely to be leave HREE-enriched apatite, as the LREE have been stripped away.

Inferred fluid composition

The composition of the altering fluid can be inferred from the chemistry of the precipitating minerals and from the geochemical behavior of certain elements. The presence of F, P, C, Ca, and the REE are attested by the crystallization of apatite and synchysite. However, the presence of Cl, which is considered the most likely complexing agent in REE-bearing hydrothermal systems (e.g., Migdisov and Williams-Jones 2014), is only inferred. Nevertheless, comparison with experimental dissolution-reprecipitation of apatite with different fluids can be used to

"fingerprint" fluid chemistry in natural examples (Harlov 2015). Unlike the majority of natural and experimental examples of dissolution-reprecipitation of apatite, monazite formation is not observed at Tundulu or Kangankunde. The only experimental example of where this has been observed is in the presence of NaCl or $CaCl_2$ (Harlov and Förster 2003). These experiments were conducted at temperatures of 900 °C, although behavior at high temperature is likely to be replicated by lower temperature fluid (Harlov 2015). The absence of monazite as a dissolution product therefore provides circumstantial evidence of Cl activity in the hydrothermal fluid, supporting the inference of REECl complexes transporting and fractionating the REE. The presence of fluid inclusions could provide further evidence for this but unfortunately none have yet been found.

IMPLICATIONS

This study provides an example of dissolution-reprecipitation, a common process in many hydrothermal systems, but rarely identified in apatite in carbonatite. Dissolution at Tundulu and Kangankunde occurs in an unusual core-outward manner, and may be due to the lower stability of "original" CO_3-bearing apatite. The REE concentrations of the turbid apatite cores (reactant apatite) are HREE enriched and the clear apatite rims (product apatite) are LREE-enriched, with apatite crystallization followed by synchysite-(Ce). The absence of monazite during dissolution-reprecipitation of apatite implies the presence of Cl-bearing fluids. It is proposed that the difference in REE distribution, with paragenesis, is caused by the relatively greater stability of LREE-chloride complexes. This leads to the preferential transport of the LREE away from the apatite cores, during dissolution, and the passive enrichment of HREE.

This study provides a geological example, in carbonatite-derived hydrothermal systems, supporting the experimentally determined stability of REE-chloride complexes (Migdisov and Williams-Jones 2014). This implies that HREE enrichment, important for increasing the value of REE deposits, is possible in carbonatite-hosted REE deposits. However, because the LREE-product is rapidly re-precipitated on the apatite rim, the bulk REE contents are likely to remain LREE-enriched. Nevertheless, if fluid activity is sufficiently high, then it may be possible that the LREE are completely removed from the apatite and re-precipitated later in the paragenetic sequence as LREE-fluorcarbonates. This may be occurring where HREE-enriched apatite from carbonatites has been reported with no LREE-rich overgrowth [e.g., Sukulu, Uganda (Ting et al. 1994) and Songwe, Malawi (Broom-Fendley et al. 2013)].

ACKNOWLEDGMENTS

REFERENCES CITED

Appleton, J.D. (1994) Direct-application fertilizers and soil amendments—appropriate technology for developing countries? In S.J. Mathers and A.J.G. Notholt, Eds.

Industrial Minerals in Developing Countries. AGID Report Series Geosciences in International Development, 18, 223–256.

Appleton, J.D., Styles, M.T., Chisale, R.T.K., Hardcastle, P.D., Sitaube, L.A., and Syers, J.K. (1991) Potential use of phosphate resources from African carbonatites as low-cost direct-application fertilizers. In D.A. Stow and D.J.C. Laming, Eds., Geoscience in Development, AGID Report 14, p. 181–190. Balkema, Rotterdam, Netherlands.

Ayers, J.C., and Watson, E.B. (1991) Solubility of apatite, monazite, zircon, and rutile in supercritical aqueous fluids with implications for subduction zone geochemistry. Philosophical Transactions of the Royal Society of London, Series A: Physical and Engineering Sciences, 335, 365–375.

Binder, G., and Troll, G. (1989) Coupled anion substitution in natural carbon-bearing apatites. Contributions to Mineralogy and Petrology, 101, 394–401.

Brassinnes, S., Balaganskaya, E., and Demaiffe, D. (2005) Magmatic evolution of the differentiated ultramafic, alkaline and carbonatite intrusion of Vuoriyarvi (Kola Peninsula, Russia). A LA-ICP-MS study of apatite. Lithos, 85, 76–92.

Brigatti, M.F., Malfererrari, D., Medici, L., Ottolini, L., and Poppi, L. (2004) Crystal chemistry of apatites from the Tapira carbonatite complex, Brazil. European Journal of Mineralogy, 16, 677–685.

Broom-Fendley, S., Wall, F., Brady, A.E., Gunn, A.G., Chenery, S.R., and Dawes, W. (2013) Carbonatite-hosted late-stage apatite as a potential source of the heavy rare earth elements. SGA Conference Abstracts, 4, 1694–1698.

Bühn, B., Wall, F., and Le Bas, M. (2001) Rare-earth element systematics of carbonatitic fluorapatites, and their significance for carbonatite magma evolution. Contributions to Mineralogy and Petrology, 141, 572–591.

Chen, W., and Simonetti, A. (2013) In-situ determination of major and trace elements in calcite and apatite, and U–Pb ages of apatite from the Oka carbonatite complex: Insights into a complex crystallization history. Chemical Geology, 353, 151–172.

Dallas, S., Laval, M., and Malunga, G.W.P. (1987) Evaluation of known mineral deposits. Bureau de Recherches Géologiques et Minières, Orleans, France, 113 pp. (unpublished).

Dunham, A.C., and Wilkinson, F.C.F. (1978) Accuracy, precision and detection limits of energy-dispersive electron-microprobe analyses of silicates. X-ray Spectrometry, 7, 50–56.

Engvik, A.E., Golla-Schindler, U., Berndt, J., Austrheim, H., and Putnis, A. (2009) Intragranular replacement of chlorapatite by hydroxy-fluor-apatite during metasomatism. Lithos, 112, 236–246.

European Commission (2014) Report on critical raw materials for the EU, report of the ad hoc working group on defining critical raw materials. Technical report, available at http://ec.europa.eu/DocsRoom/documents/10010/attachments/1/translations/en/renditions/native. (Archived by WebCite at http://www.webcitation.org/6cJu6Nnpj.)

Fleet, M.E., Liu, X., and King, P.L. (2004) Accommodation of the carbonate ion in apatite: An FTIR and X-ray structure study of crystals synthesized at 2–4 GPa. American Mineralogist, 89, 1422–1432.

Garson, M. (1962) The Tundulu carbonatite ring-complex in southern Nyasaland. Memoirs of the Geological Survey of Malawi, 2.

———— (1965) Carbonatites in southern Malawi. Bulletin of the Geological Survey of Malawi, 15.

Garson, M., and Campbell Smith, W. (1965) Carbonatite and agglomeratic vents in the western Shire Valley. Memoirs of the Geological Survey of Malawi, 3.

Gunn, A.G., Ed. (2014) Critical Metals Handbook. Wiley, New York.

Haas, J.R., Shock, E.L., and Sassani, D.C. (1995) Rare earth elements in hydrothermal systems: estimates of standard partial molal thermodynamic properties of aqueous complexes of the rare earth elements at high pressures and temperatures. Geochimica et Cosmochimica Acta, 59, 4329–4350.

Harlov, D.E. (2015) Apatite: a fingerprint for metasomatic processes. Elements, 11, 171–176.

Harlov, D.E., and Förster, H.-J. (2003) Fluid-induced nucleation of (Y+REE)-phosphate minerals within apatite: Nature and experiment. Part II. Fluorapatite. American Mineralogist, 88, 1209–1229.

Harlov, D.E., Andersson, U.B., Förster, H.-J., Nyström, J.O., Dulski, P., and Broman, C. (2002a) Apatite-monazite relations in the Kiirunavaara magnetite-apatite ore, northern Sweden. Chemical Geology, 191, 47–72.

Harlov, D.E., Förster, H.-J., and Nijland, T.G. (2002b) Fluid-induced nucleation of REE-phosphate minerals in apatite: Nature and experiment. Part I. Chlorapatite. American Mineralogist, 87, 245–261.

Harlov, D.E., Wirth, R., and Förster, H.-J. (2005) An experimental study of dissolution-reprecipitation in fluorapatite: fluid infiltration and the formation of monazite. Contributions to Mineralogy and Petrology, 150, 268–286.

Hogarth, D. (1989) Pyrochlore, apatite and amphibole: Distinctive minerals in carbonatite. In K. Bell, Ed., Carbonatites: Genesis and evolution, p. 105–148, Unwin Hyman, London.

Holt, D.N. (1965) The Kangankunde Hill rare earth prospect. Bulletin of the Geological Survey of Malawi, 20.

Hornig-Kjarsgaard, I. (1998) Rare earth elements in sovitic carbonatites and their mineral phases. Journal of Petrology, 39, 2105–2121.

Hughes, J.M., and Rakovan, J.F. (2015) Structurally robust, chemically diverse: apatite and apatite supergroup minerals. Elements, 11, 165–170.

Ihlen, P.M., Schiellerup, H., Gautneb, H., and Skår, Ø. (2014) Characterization of apatite resources in Norway and their REE potential—a review. Ore Geology Reviews, 58, 126–147.

Kapustin, I. (1980) Mineralogy of Carbonatites. Amerind, New Delhi.

Krause, J., Harlov, D.E., Pushkarev, E.V., and Brügmann, G.E. (2013) Apatite and clinopyroxene as tracers for metasomatic processes in nepheline clinopyroxenites of Uralian-Alaskan-type complexes in the Ural Mountains, Russian Federation. Geochimica et Cosmochimica Acta, 121, 503–521.

Le Bas, M. (1989) Diversification of carbonatite. In K. Bell, Ed., Carbonatites: Genesis and evolution, p. 428–427 Unwin Hyman, London.

Le Bas, M., and Handley, C. (1979) Variation in apatite composition in ijolitic and carbonatitc igneous rocks. Nature, 279, 54–56.

Liu, Y., and Comodi, P. (1993) Some aspects of the crystal-chemistry of apatites. Mineralogical Magazine, 57, 709–719.

Mariano, A.N., and Mariano, A. (2012) Rare earth mining and exploration in North America. Elements, 8, 369–376.

McDonough, W., and Sun, S. (1995) The composition of the Earth. Chemical Geology, 120, 223–253.

Migdisov, A.A., and Williams-Jones, A. (2008) A spectrophotometric study of Nd (III), Sm (III) and Er (III) complexation in sulfate-bearing solutions at elevated temperatures. Geochimica et Cosmochimica Acta, 72, 5291–5303.

——— (2014) Hydrothermal transport and deposition of the rare earth elements by fluorine-bearing aqueous liquids. Mineralium Deposita, 49, 987–997.

Migdisov, A.A., Williams-Jones, A., and Wagner, T. (2009) An experimental study of the solubility and speciation of the rare earth elements (III) in fluoride and chloride-bearing aqueous solutions at temperatures up to 300 °C. Geochimica et Cosmochimica Acta, 73, 7087–7109.

Ngwenya, B.T. (1991) Magmatic and post-magmatic geochemistry of phosphorus and rare earth elements in carbonatites. Ph.D. thesis, Reading University, U.K.

——— (1994) Hydrothermal rare earth mineralisation in carbonatites of the Tundulu complex, Malawi: Processes at the fluid/rock interface. Geochimica et Cosmochimica Acta, 58, 2061–2072.

Pan, Y., and Fleet, M.E. (2002) Compositions of the apatite-group minerals: Substitution mechanisms and controlling factors. Reviews in Mineralogy and Geochemistry, 48, 13–49.

Putnis, A. (2002) Mineral replacement reactions: from macroscopic observations to microscopic mechanisms. Mineralogical Magazine, 66, 689–708.

——— (2009) Mineral replacement reactions. Reviews in Mineralogy and Geochemistry, 70, 87–124.

Putnis, C.V., and Ruiz-Agudo, E. (2013) The mineral–water interface: where minerals react with the environment. Elements, 9, 177–182.

Robertson, S. (1999) BGS rock classification scheme volume 2. Classification of metamorphic rocks. British Geological Survey research report, RR 99-02, available at http://www.bgs.ac.uk/bgsrcs/.

Ruiz-Agudo, E., Putnis, C.V., and Putnis, A. (2014) Coupled dissolution and precipitation at mineral–fluid interfaces. Chemical Geology, 383, 132–146.

Sheard, E., Williams-Jones, A., Heilgmann, M., Pederson, C., and Trueman, D. (2012) Controls on the concentration of zirconium, niobium, and the rare earth elements in the Thor Lake rare metal deposit, Northwest Territories, Canada. Economic Geology, 107, 81–104.

Stock, M.J., Humphreys, M.C.S., Smith, V.C., Johnson, R.D., Pyle, D.M., and EIMF (2015) New constraints on electron-beam induced halogen migration in apatite. American Mineralogist, 100, 281–293.

Stoppa, F., and Liu, Y. (1995) Chemical composition and petrogenetic implications of apatites from some ultra-alkaline Italian rocks. European Journal of Mineralogy, 7, 391–402.

Stormer, J., Pierson, M.L., and Tacker, R.C. (1993) Variation of F and Cl X-ray intensity due to anisotropic diffusion in apatite. American Mineralogist, 78, 641–648.

Styles, M.T. (1988) A preliminary report on the mineralogy of the Tundulu and Songwe carbonatite complexes, Malawi. British Geological Survey, Nottingham, 10pp. (WG/88/006) (unpublished), available at http://nora.nerc.ac.uk/511266.

Styles, M.T., and Young, B.R. (1983) Fluocerite and its alteration products from the Afu Hills, Nigeria. Mineralogical Magazine, 47, 41–46.

Ting, W., Burke, E.A., Rankin, A.H., and Woolley, A.R. (1994) Characterisation and petrogenetic significance of CO_2, H_2O and CH_4 fluid inclusions in apatite from the Sukulu Carbonatite, Uganda. European Journal of Mineralogy, 6, 787–803.

Wall, F. (2000) Mineral chemistry and petrogenesis of rare earth-rich carbonatites with particular reference to the Kangankunde carbonatite, Malawi. Ph.D. thesis, Univeristy of London, U.K.

——— (2014) Rare earth elements. In A.G. Gunn, Ed., Critical Metals Handbook, pp. 312–339. Wiley, New York.

Wall, F., and Mariano, A. (1996) Rare earth minerals in carbonatites: A discussion centred on the Kangankunde carbonatite, Malawi. In A. Jones, F. Wall, and C.T. Williams, Eds., Rare Earth Minerals: Chemistry Origin and Ore Deposits, pp. 193–226. Chapman and Hall, London.

Walter, A.-V., Nahon, D., Flicoteaux, R., Girard, J., and Melfi, A. (1995) Behaviour of major and trace elements and fractionation of REE under tropical weathering of a typical apatite-rich carbonatite from Brazil. Earth and Planetary Science Letters, 136, 591–602.

Walters, A., Goodenough, K., Hughes, H., Roberts, N., Gunn, A., Rushton, J., and Lacinska, A. (2013) Enrichment of rare earth elements during magmatic and post-magmatic processes: A case study from the Loch Loyal Syenite Complex, northern Scotland. Contributions to Mineralogy and Petrology, 166, 1177–1202.

Wang, L.-X., Marks, M.A., Wenzel, T., Von Der Handt, A., Keller, J., Teiber, H., and Markl, G. (2014) Apatites from the Kaiserstuhl Volcanic Complex, Germany: new constraints on the relationship between carbonatite and associated silicate rocks. European Journal of Mineralogy, first published online, doi: 10.1127/0935-1221/2014/0026-2377.

Williams-Jones, A., Migdisov, A.A., and Samson, I. (2012) Hydrothermal mobilization of the rare earth elements: A tale of "Ceria" and "Yttria". Elements, 8, 355–360.

Woolley, A. (2001) Alkaline rocks and carbonatites of the World. Part 3: Africa. The Geological Society, London, 1.

Xu, C., Kynicky, J., Chakhmouradian, A.R., Campbell, I.H., and Allen, C.M. (2010) Trace-element modeling of the magmatic evolution of rare-earth rich carbonatite from the Miaoya deposit, Central China. Lithos, 118, 145–155.

Zaitsev, A.N., Williams, C.T., Jeffries, T.E., Strekopytov, S., Moutte, J., Ivashchenkova, O.V., Spratt, J., Petrov, S.V., Wall, F., Seltmann, R., and Borozdin, A.P. (2015) Rare earth elements in phoscorites and carbonatites of the Devonian Kola Alkaline Province, Russia: Examples from Kovdor, Khibina, Vuoriyarvi and Turiy Mys complexes. Ore Geology Reviews, 64, 477–498.